Loading-rate dependent Poisson's ratio of polyurethane auxetic foams at different loading strains; a user-defined material model and experimental verification

Ali Behbahani[a], Amir Nourani[a,*]

a. Department of Mechanical Engineering, Sharif University of Technology, Azadi Ave, Tehran, Iran

Corresponding author[*]: Amir Nourani

Email: nourani@sharif.edu | Tel: +98(21) 6616-5687 , Mobile Number: +98(913) 328-4163 | Address: Department of Mechanical Engineering, Sharif University of Technology, Azadi St., Tehran, Iran (Islamic Republic of), Postal Code: 1458889694

Author: Ali behbahani

Email: abehbah@vols.utk.edu | Tel: +1(865) 232-0841 | Address: Department of Mechanical Engineering, Sharif University of Technology, Azadi St., Tehran, Iran (Islamic Republic of), Postal Code: 1458889694

Abstract

This study investigated the combined effects of loading rate and applied strain on the behavior of auxetic materials and developed a user-defined material model to capture these effects during loading. First, test specimens were made of conventional polyurethane foams according to *ASTM D-3574*; then, with a thermo-mechanical process, the conventional foam was converted to auxetic polyurethane foam. Tensile experiments were conducted by applying different strains (i.e., *10*, *40*, and *80*%) and loading rates (i.e., *0.01*, *1*, and *5* s^{-1}). Displacements were tracked during the tests by digital image correlation. Statistical analysis using analysis of variance (ANOVA) showed that both strain and loading rate significantly affect Poisson's ratio ($p<0.0001$). It was also found that transient strain auxeticity (TSA) depends on the applied loading

rate. The user-defined material was developed from the experiments and used in a finite element model (FEM) to capture Poisson's ratio variations because of changing loading circumstances. The model's predictive ability (i.e., the model's validity) was examined by performing different experiments (i.e., different from those used for developing the model), showing a maximum difference of *10%* compared to measured Poisson’s ratio-strain curves from experiments.

Keywords:

Auxetic, Foam, Poisson’s ratio, Strain, Loading rate, Strain rate, Experiments, FEM, statistical analysis

Funding sources:

This research did not receive any specific grant from funding agencies in the public, commercial, or not-for-profit sectors.

1- Introduction

A material with a negative Poisson's ratio (NPR) is termed auxetic material. In 1987, the first auxetic foam was created [1]. Auxetic foams have exhibited distinct features such as resistance to indentation due to increased shear modulus with respect to regular foams [2], [3], [4], [5], [6]. These materials have also shown a superior ability to absorb vibrations [7], [8] and microwaves [9], [10] as compared to conventional foams. Because of the aforementioned qualities, auxetic materials have a broad variety of uses, including personal protective equipment [11] and energy absorption [12], [13], [14], [15]. The proper comfort, high energy absorption, and low weight of auxetic materials have prompted manufacturers of sports protective equipment to actively explore these materials to be used in shoes, gloves, and helmets[16]. As a result, to make use of these materials in various applications and

throughout their working lifespan, the dependency of Poisson's ratio (ν) on loading circumstances needs to be determined.

The magnitude of applied strain has been found as a key factor affecting the ν. For instance, variations of ν in conventional polyurethane foam have shown a significant dependency on the strain[17], [18], [19]; i.e., ν increased by about *50%* from *0.3* to *0.58* during a compressive test[20]. Refs. [21], [22], [23], [24] found that in an auxetic polyurethane foam material by increasing the amount of strain, negative Poisson's ratio (NPR) began to increase due to the reduction in the amount of residual strains, i.e., produced in the thermo-mechanical process, converting a conventional foam to an auxetic one, and after a specific strain (i.e., transition strain), the material showed a positive ν like a conventional foam; the ν was about *-0.22* at the beginning of loading, and after applying a strain of *100%*, [21] the ν value became *0.02*; i.e. ν value increased by almost *110%*. Ref. [15], [25], [26] found that ν changed for auxetic structure by changing the applied strain in tensile loading.

In addition to the amount of strain, the applied loading rate has been found to influence the ν in polyurethane foams [27], [28]. Also, for auxetic polyurethane foams studies revealed that increasing the loading rate was found to change the NPR with a faster rate (i.e., at a smaller strain) compared to lower loading rates, moving toward the positive amount of ν [29], [30], [31]. In other words, by increasing the rate of loading, the residual strain, i.e., produced in the thermo-mechanical process, changed with a sharper trend; e.g., the initial ν for a specimen was *0.08*, and it remained in the auxetic domain by applying a *70*% strain at $\dot{\varepsilon} = 0.01\ s^{-1}$, while, the same specimen turned into a conventional foam when loaded under a ε_{11} of *50*% at $\dot{\varepsilon} = 1\ s^{-1}$[29].

The studies mentioned above performed some experiments and did not develop a model to predict the material behavior during loading at different loading rates. The experiments were conducted under compressive loading, which can show a different behavior compared to tensile loading conditions. Furthermore, none of those studies investigated the simultaneous effects of strain and loading rate (i.e., interaction between these two loading parameters) on the variations of ν. The current study, therefore, investigates the combined effects of strain and loading rate on variations of ν for tensile loading. Design of experiments is performed, and *36* tests are conducted under various loading scenarios, i.e., strain values between *0* and *80%* and loading rates ranging from *0.01* to *5* s^{-1}. Statistical analysis is used to determine the main and interactional effects of the loading parameters. Based on the experimental results, a user-defined material code with adaptive ν is developed using finite element modeling (FEM). We hypothesized that this adaptive FEM could predict the mechanical behavior of the auxetic foam under different loading conditions, i.e., different from those performed to develop the code.

2- Materials and Method

2-1 Design of experiments

In the present study, three ε_{11} levels which were *10*, *40*, and *80%*, and four $\dot{\varepsilon}_{11}$ values of *0.01*, *0.1*, *1*, and *5* s^{-1} were examined. The design of experiments was done based on a general full factorial approach giving twelve loading scenarios. To ensure repeatability, each test was repeated three times, and, hence, a total number of *36* experiments were conducted.

2-2 Specimen preparation

A conventional polyurethane foam with a density of *20* $\frac{kg}{m^3}$ and an initial thickness of *5* mm was utilized to make the auxetic foam following the approach of [32]. The specimen geometry was generated by *ASTM D-3574 Test E*, as seen in Figure 1a. A thermo-mechanical treatment was used to convert the conventional foam into an auxetic foam; first, the specimen was placed in a specially designed pressure mechanism and compressed from *5* to *2 mm* (Figure 1b). After that, the entire system was exposed to heat, i.e., at a softening temperature of $200°C$ for *45 min*. The foam was then cooled down to room temperature for *10 min*. Finally, the system was exposed to $150°C$ for *45 min* to finalize the microstructure shaping into an auxetic foam.

2-3 Test setup

A servo-hydraulic Machine (i.e., *Zwick-Roell Amsler HTC 25-400*) with a load cell having a capacity of *20 kN* and accuracy of *1 N* was used to load the specimen fixed on a specially designed fixture to prevent slippage during testing (see Figure 2a). The crosshead speed and effective length of the specimen (i.e., the distance between the two jaws of the fixture) were adjusted in the way that the desired $\dot{\varepsilon}_{11}$ was achieved, e.g., for $\dot{\varepsilon}_{11}$ of *0.01* s^{-1} with the specimen effective length of *35 mm*, the crosshead speed was *0.35 mm.* s^{-1}. Digital image correlation was used to measure deformations in directions *1* (i.e., loading direction), *2*, and *3* (i.e., perpendicular to the loading direction). To do this, a dark porous pattern was made on the specimen. A digital camera with a maximum resolution of *4K* and a maximum frame per second of *240* was used to record the deformation of the specimens while they were being loaded. A source of white light in front of the specimen at a *45 cm* distance aided capture high-quality images. To achieve uniform loading during the experiments, before starting the

test, a grid image was captured, the upper and lower parts of the fixture were parallel, and the position of the test specimen in the fixture was ensured. One grid image was shown in Figure 2b. The video recordings were imported to the software (GOM Correlate software, GOM Metrology Co., Schmitzstraße 2, 38122 Braunschweig, Germany) for image processing. The axial and transversal strains (ε_{11}, ε_{13}, and ε_{23}) were measured by three digital extensometers for each direction that were specified in the software. The magnitude of strain for longitudinal and transversal directions was obtained by taking the average of the values from the extensometers in each direction. The facet size of these extensometers was *17* pixels, and the computation method for tracking ε with these extensometers was based on more point matches against the previous frame of the video. Table 1 summarizes the tests performed in the current study.

2-4 Statistical analysis

A two-sided analysis of variance (ANOVA) with a confidence interval of *95%* was used to evaluate the significance of changes in mean values of ν (obtained from repeated tests) with variations of ε_{11} and/or $\dot{\varepsilon}_{11}$.

2-5 Finite element model (FEM)

A FEM was built in Abaqus software with a general static solver. The boundary conditions and loading on the specimen were applied in the model (see Figure 3a) to represent the testing configuration as depicted in Figure 2. A continuum three-dimensional element with a size of *0.2 mm* was employed based on a mesh-size sensitivity analysis. Since the ν changes with the applied ε_{11} and $\dot{\varepsilon}_{11}$ of loading, a user-defined material code was developed based on the test findings to obtain a constitutive model with an adaptive ν. As a result of this adaptive code, ν was defined

as a function of ε_{11} and $\dot{\varepsilon}_{11}$. The flowchart of Figure 4 shows the procedure conducted to develop the code. This code was then used to predict the deformation of auxetic foams in different loading cases.

2-6 Material model

As a result of a linear stress-strain curve, Hook's model was used in this study to reduce the experiments and computational costs in comparison with nonlinear models like orthotropic Fung's model, which has *18* experimental coefficients to calibrate the model. Calibration experiments were conducted to obtain Hook's model constants. As will be shown in Section 3-3, those experiments exhibited a good correlation (at least *90%*) with Hook's model using the adaptive Poisson's ratio. The model code was written in FORTRAN *77* language with adaptive ν in different directions during loading. The code was then coupled with Abaqus software to predict the material behavior during loading. Finally, the model predictions were compared with experimental results (other than the calibration experiments) to validate the FEM. Also, Table 2 shows the material properties used in the simulation. Hook's law can be written in the following form (2-7):

$$\begin{bmatrix} \varepsilon_{11} \\ \varepsilon_{22} \\ \varepsilon_{33} \\ \varepsilon_{12} \\ \varepsilon_{13} \\ \varepsilon_{23} \end{bmatrix} = \begin{bmatrix} \frac{1}{E_1} & \frac{-\nu_{21}}{E_2} & \frac{-\nu_{31}}{E_3} & 0 & 0 & 0 \\ \frac{-\nu_{12}}{E_1} & \frac{1}{E_2} & \frac{-\nu_{32}}{E_3} & 0 & 0 & 0 \\ \frac{-\nu_{13}}{E_1} & \frac{-\nu_{23}}{E_2} & \frac{1}{E_3} & 0 & 0 & 0 \\ 0 & 0 & 0 & \frac{1}{2G_{12}} & 0 & 0 \\ 0 & 0 & 0 & 0 & \frac{1}{2G_{13}} & 0 \\ 0 & 0 & 0 & 0 & 0 & \frac{1}{2G_{23}} \end{bmatrix} \times \begin{bmatrix} \sigma_{11} \\ \sigma_{22} \\ \sigma_{33} \\ \sigma_{12} \\ \sigma_{13} \\ \sigma_{23} \end{bmatrix} \quad (2\text{-}7)$$

In the FEM developed, the compliance matrix will update with changing ν in different directions based on Equation (2 to 7).

3-Results

3-1 Manufacturing

The conventional foam was converted to auxetic foam with a thermo-mechanical process as explained in Section 2-2. To ensure repeatability of the manufacturing process, the procedure was performed on *63* specimens. After the thermo-mechanical process [32] the auxetic foam's thickness was reduced by *46%* in comparison with conventional foam's thickness (from *5 mm to 2.7 mm* see Figure 5) with the coefficient of variant (CoV) of *1.5%* for *63* specimens. Furthermore, the measured ν for different specimens had a CoV of *4%* as will be shown in Section 3-2.

As is obvious in Figure 6, the walls of the foam's microcell buckled in such a way that the mean perimeter of each cell decreased by about *50%* (from *1.76 mm to 0.88 mm*) and the area reduced by almost *60%* (from *0.18 mm*^{2} to *0.06 mm*^{2}).

3-2 Experimental results for conventional foam (Class A)

As indicated in Table 1, Class A tests (i.e., Cases 1-12, termed as control tests) were conducted to examine variations of ν for conventional foams under different loading conditions. As you can see in Figures 7a-c the ν always had a positive value for $\dot{\varepsilon}_{11}$ = *0.01* to *1 s*$^{-1}$ the ν had three regions which started with a descended region after observed an ascended region and finally a plateau region was observed. On the other hand, the ν for $\dot{\varepsilon}_{11}$ = *5 s*$^{-1}$ has an ascended behavior in all strains.

3-3 Experimental results for calibration auxetic foams (Class B)

ʌ

Figure 8a shows the engineering stress-strain curve for auxetic foams loaded under different $\dot{\varepsilon}_{11}$. Also, Poisson's ratios of different directions for $\dot{\varepsilon}_{11}$= *0.01 s*$^{-1}$ are depicted in Figure 8b which showed a good correlation in their trend with the literature [33], [34].

3-4 Experimental results for validation auxetic foams (Class C)

3-4-1 Effect of ε_{11} on ν_{13}

Figs. 9a-c show the ν_{13} variations for different loading conditions. As it is obvious from Figure 9, The analysis reveals significant variations in ν_{13} for different combinations of ε_{11} and $\dot{\varepsilon}_{11}$ values:

1. For $\dot{\varepsilon}_{11}$ = *0.01*:
    - A substantial *225%* increase was observed when comparing ε_{11} = *10%* to ε_{11} = *40%*.
    - An even more substantial *378%* increase was noted between ε_{11} = *10%* and ε_{11} = *80%*.
2. For $\dot{\varepsilon}_{11}$ = *0.1*:
    - A *121%* increase was observed when comparing ε_{11}= *10%* to ε_{11}= *40%*.
    - A *142%* increase was observed when comparing ε_{11} = *10%* to ε_{11}= *80%*.
3. For $\dot{\varepsilon}_{11}$ = *1*:

- A *105%* increase was noted for ε_{11} = *40%* compared to ε_{11} = *10%*.
- A *157%* increase was observed for ε_{11} = *80%* compared to ε_{11} = *10%*.

4. For $\dot{\varepsilon}_{11}$ = *5*:
   - A *21%* increase was seen for ε_{11} = *40%* compared to ε_{11} = *10%*.
   - A *6%* increase was observed for ε_{11} = *80%* compared to ε_{11} = *10%*.

3-4-2 Effect of $\dot{\varepsilon}_{11}$ on ν_{13}

The trend of ν_{13} for auxetic foam during different loading conditions changed, as is obvious from Figures 10a-d. The overall variation pattern of ν_{13} could be categorized into three regions. In the first region, ν_{13} starts to decrease until its min value. By increasing the loading rate, this region decreases (ε_{11} = *13%* to ε_{11} = *0*). The second region has a positive slope which means that ν_{13} starts to increase and convert from an auxetic foam to a conventional foam after reaching a certain strain (meet its transient strain auxeticity). This region continues until the ν_{13} reaches its max value on those loading conditions. This region was also affected by the loading rate, and by increasing the loading rate, the region occurs at a smaller domain of strain (ε_{11} = *47%* to *22%*). The third region is the plateau region which means ν_{13} reaches its max value, and by increasing strain, the ν_{13} has a semi-constant value. By increasing the loading rate, this region was increased, which implies that by increasing the loading rate, the ν_{13} reaches its max value at a smaller strain (ε_{11} =*20%* to *57%*).

3-5 Statistical analysis for ν_{13}

Statistical analysis shows that all parameters, including ε_{11} and $\dot{\varepsilon}_{11}$, and the interaction between them, can affect the variations of ν_{13}. Based on this analysis, ε_{11} is the most effective parameter and after that, the interaction between ε_{11} and $\dot{\varepsilon}_{11}$, and $\dot{\varepsilon}_{11}$ are located, respectively, in descending order of influence. Experiments showed that, in addition to the amount of ε_{11} applied, auxetic foam ν behavior was also influenced by the $\dot{\varepsilon}_{11}$. Figure 11 indicates that the foam with a ε_{11} = *10%* had the lowest ν_{13} and that this value rises with increasing ε_{11}, such that the foam with ε_{11} = *80%* showed the highest Poisson ratio. Increasing $\dot{\varepsilon}_{11}$ acted the same way as increasing the amount of ε_{11}; the value of the ν moved toward positive values by elevating either ε_{11} or $\dot{\varepsilon}_{11}$. As shown in Figure 11, at the $\dot{\varepsilon}_{11}$ of *5* s^{-1}, ν always had a positive value. This foam's behavior took place due to the increasing amount of ε_{11} on the bucked walls of the honeycomb structure of auxetic foam, which started to open, and with increasing the rate of loading, this phenomenon occurred in a shorter duration.

The ANOVA statistical analysis results revealed that the effect of changing the ε_{11} from *10%* to *40%* had the most significant effect on changing the ν. Additionally, the highest slope of ν changes with ε_{11} is observed for the $\dot{\varepsilon}_{11}$ of *5* s^{-1} (see Figure 12a). Moreover, as Figure 12b shows, it was observed that the interaction of these two loading factors in quasi-static $\dot{\varepsilon}_{11}$ is significant, while increasing the $\dot{\varepsilon}_{11}$, the interaction effect noticeably reduced.

3-6 Statistical analysis for TSA

The statistical study of TSA illustrates that strain, $\dot{\varepsilon}_{11}$, and the interaction of these two loading factors, all, had an influence on the variations of ν, and that the ε_{11}

magnitude had the most significant effect in this analysis. After the ε_{11} effect, the interaction between parameters and $\dot{\varepsilon}_{11}$ effects were positioned, respectively. Experiments showed that the foam's TSA also depends on the amount of ε_{11} and $\dot{\varepsilon}_{11}$, with increasing the ε_{11} the TSA of the foam decreased, moreover, for $\dot{\varepsilon}_{11}$ = *0.01* to *1* s^{-1} The TSA has the same value for ε_{11}= *80%* but for the ε_{11}= *40%* the TSA doesn't follow a predictable pattern, as seen in Figure 13. Also, Figure 13 shows that for the $\dot{\varepsilon}_{11}$= *5* s^{-1} no TSA is observed, and the foam does not show auxetic behavior

The same statistical analysis for TSA shows that increasing $\dot{\varepsilon}_{11}$ = *1* to *5* s^{-1} had a critical role in the foam's TSA behavior by a rapid change in TSA, making it zero at the beginning of loading. Also, the interaction between ε_{11} and $\dot{\varepsilon}_{11}$ had the same trend as did ν, i.e., the interaction between these two loading parameters in quasi-static loading conditions had a more significant effect on TSA compared to dynamic loading conditions. Figures 14a-b show the trends explained above.

3-7 Finite element analysis

A strain-rate dependent user-defined material code in FEM was developed to capture variations of Poisson's ratio for the applied strains using the measurements recorded for calibration experiments. Equations (3-1 to 3-12) (i.e., lines fitted on the calibration experiments in Figs. 10a-d give the estimated linear relationships between Poisson's ratio and applied strain for different loading rates. These lines had an overall accuracy of within R-square = *90%* compared to experimental results. For the non-auxetic direction of the material Equations (3-13 to 3-16) define the behavior of Poisson's ratio for different strain rates.

$$\dot{\varepsilon}=0.01\left(s^{-1}\right):\begin{cases}\nu_{13}=-0.0308\varepsilon_{11}-0.119 & 0\le\varepsilon_{11}<5.6\\ \nu_{13}=1.7\varepsilon_{11}-0.166 & 5.6\le\varepsilon_{11}\le100\end{cases} \tag{3-1}$$

$$\dot{\varepsilon}=0.1\left(s^{-1}\right):\ \{\nu_{13}=-0.044\varepsilon_{11}+0.0024 \qquad 0\le\varepsilon_{11}\le10 \tag{3-2}$$

$$\dot{\varepsilon}=1\left(s^{-1}\right):\quad\begin{cases}\nu_{13}=-0.0735\varepsilon_{11}-0.0472 & 0\le\varepsilon_{11}<6.0\\ \nu_{13}=0.0481\varepsilon_{11}-0.7796 & 6.0\le\varepsilon_{11}<8.3\\ \nu_{13}=-0.0311\varepsilon_{11}-0.1246 & 8.3\le\varepsilon_{11}\le10\end{cases} \tag{3-3}$$

$$\dot{\varepsilon}=5\left(s^{-1}\right):\quad\begin{cases}\nu_{13}=0.1969\varepsilon_{11}+0.0704 & 0\le\varepsilon_{11}<2.0\\ \nu_{13}=-0.1261\varepsilon_{11}+0.7113 & 2\le\varepsilon_{11}<3.3\\ \nu_{13}=0.053\varepsilon_{11}+0.1246 & 3.3\le\varepsilon_{11}<6.0\\ \nu_{13}=0.44 & 6.0\le\varepsilon_{11}\le10\end{cases} \tag{3-4}$$

$$\dot{\varepsilon}=0.01\left(s^{-1}\right):\begin{cases}\nu_{13}=-0.0367\varepsilon_{11}-0.0076 & 0\le\varepsilon_{11}<3.7\\ \nu_{13}=0.0064\varepsilon_{11}-0.166 & 3.7\le\varepsilon_{11}\le40\end{cases} \tag{3-5}$$

$$\dot{\varepsilon}=0.1\left(s^{-1}\right):\begin{cases}\nu_{13}=-0.2053\varepsilon_{11}+0.03 & 0\le\varepsilon_{11}<3.4\\ \nu_{13}=0.0406\varepsilon_{11}-0.7966 & 3.4\le\varepsilon_{11}<16.65\\ \nu_{13}=0.0184\varepsilon_{11}-0.4267 & 16.65\le\varepsilon_{11}<27.5\\ \nu_{13}=0.08 & 27.5\le\varepsilon_{11}\le40\end{cases} \tag{3-6}$$

$$\dot{\varepsilon}=1\left(s^{-1}\right):\quad\begin{cases}\nu_{13}=-0.4954\varepsilon_{11}-0.0864 & 0\le\varepsilon_{11}<0.83\\ \nu_{13}=0.016\varepsilon_{11}-0.5095 & 0.83\le\varepsilon_{11}<33.15\\ \nu_{13}=0.02 & 33.15\le\varepsilon_{11}\le 40\end{cases}\qquad(3\text{-}7)$$

$$\dot{\varepsilon}=5\left(s^{-1}\right):\quad\begin{cases}\nu_{13}=-0.109\varepsilon_{11}-0.0231 & 0\le\varepsilon_{11}<4.16\\ \nu_{13}=0.0055\varepsilon_{11}+0.4077 & 4.16\le\varepsilon_{11}<19.88\\ \nu_{13}=0.52 & 19.88\le\varepsilon_{11}\le 40\end{cases}\qquad(3\text{-}8)$$

$$\dot{\varepsilon}=0.01\left(s^{-1}\right):\begin{cases}\nu_{13}=-0.0023\varepsilon_{11}-0.0064 & 0\le\varepsilon_{11}<11.50\\ \nu_{13}=0.0084\varepsilon_{11}-0.1298 & 11.50\le\varepsilon_{11}<36.85\\ \nu_{13}=0.0022\varepsilon_{11}+0.099 & 36.85\le\varepsilon_{11}<57.37\\ \nu_{13}=-0.001\varepsilon_{11}+0.2819 & 57.37\le\varepsilon_{11}\le 80\end{cases}\qquad(3\text{-}9)$$

$$\dot{\varepsilon}=0.1\left(s^{-1}\right):\begin{cases}\nu_{13}=-0.0118\varepsilon_{11}+0.0002 & 0\le\varepsilon_{11}<8.72\\ \nu_{13}=0.0134\varepsilon_{11}-0.2193 & 8.72\le\varepsilon_{11}<32.88\\ \nu_{13}=0.0017\varepsilon_{11}+0.1687 & 32.88\le\varepsilon_{11}<61\\ \nu_{13}=-0.0014\varepsilon_{11}+0.3574 & 61\le\varepsilon_{11}\le 80\end{cases}\qquad(3\text{-}10)$$

$$\dot{\varepsilon}=1\left(s^{-1}\right):\quad\begin{cases}\nu_{13}=-0.0137\varepsilon_{11}-0.0047 & 0\le\varepsilon_{11}<10.59\\ \nu_{13}=0.0135\varepsilon_{11}-0.2935 & 10.59\le\varepsilon_{11}<35.86\\ \nu_{13}=0.191 & 35.86\le\varepsilon_{11}\le 80\end{cases}\qquad(3\text{-}11)$$

$$\dot{\varepsilon} = 5\left(s^{-1}\right): \quad \begin{cases} \nu_{13} = 0.1206\varepsilon_{11} + 0.0488 & 0 \le \varepsilon_{11} < 1.61 \\ \nu_{13} = -0.0234\varepsilon_{11} + 0.2802 & 1.61 \le \varepsilon_{11} < 5.18 \\ \nu_{13} = 0.0157\varepsilon_{11} + 0.0775 & 5.18 \le \varepsilon_{11} < 20.71 \\ \nu_{13} = 0.4025 & 20.71 \le \varepsilon_{11} < 80 \end{cases} \tag{3-12}$$

$$\dot{\varepsilon} = 0.01\left(s^{-1}\right): \quad \begin{cases} \nu_{12} = -0.0221\varepsilon_{11} + 03877 & 0 \le \varepsilon_{11} < 5.62 \\ \nu_{12} = 0.009\varepsilon_{11} + 0.2129 & 5.62 \le \varepsilon_{11} < 29.80 \\ \nu_{12} = 0.4798 & 29.80 \le \varepsilon_{11} \le 80 \end{cases} \tag{3-13}$$

$$\dot{\varepsilon} = 0.1\left(s^{-1}\right): \quad \begin{cases} \nu_{12} = -0.0171\varepsilon_{11} + 0.3906 & 0 \le \varepsilon_{11} < 7.17 \\ \nu_{12} = 0.0071\varepsilon_{11} + 0.2167 & 7.17 \le \varepsilon_{11} < 35.00 \\ \nu_{12} = 0.4753 & 35.00 \le \varepsilon_{11} \le 80 \end{cases} \tag{3-14}$$

$$\dot{\varepsilon} = 1\left(s^{-1}\right): \quad \begin{cases} \nu_{12} = -0.0091\varepsilon_{11} \mp 0.4003 & 0 \le \varepsilon_{11} < 10.40 \\ \nu_{12} = 0.0049\varepsilon_{11} + 0.2547 & 10.40 \le \varepsilon_{11} < 46.68 \\ \nu_{12} = 0.4815 & 46.68 \le \varepsilon_{11} \le 80 \end{cases} \tag{3-15}$$

$$\dot{\varepsilon} = 5\left(s^{-1}\right): \begin{cases} \nu_{12} = 0.0016\varepsilon_{11} \mp 0.4067 & 0 \le \varepsilon_{11} < 47.52 \\ \nu_{12} = 0.4827 & 47.52 \le \varepsilon_{11} \le 80 \end{cases} \tag{3-16}$$

To validate the model, the deformation of validation auxetic foams (i.e., Cases C in Table 1) measured from experiments was compared to that obtained from FEM for both auxetic direction (13) and non-auxetic direction (12). The regression was

conducted using the Weighted Interpolation method showing R-square values of *87%* and *83%* for $\dot{\varepsilon}_{11}$ = *0.05* and *0.5* s^{-1} for auxetic direction and for non-auxetic direction R-square values of *80%* and *85%* for $\dot{\varepsilon}_{11}$ = *0.05* and *0.5* s^{-1}, respectively (see Figs. 15a-b). The R-square values represent the points in the graph where the experiments and FEM models differ more from each other.

4-Discussion

This is the first study to our knowledge that investigates the simultaneous effects of tensile loading parameters (i.e., strain and loading rate) on changes in Poisson's ratio of auxetic polyurethane foams. The main objective was to first examine the existence of such influences and to develop an adaptive model to capture these effects. Significant influences of both effects were observed with the following outcomes: 1) Poisson's ratio for auxetic foam depends on the loading parameters of strain and loading rates and the interaction between them. 2) The TSA of auxetic foam was affected by the amounts of strain and loading rates and the interaction between them. 3) The developed model can successfully predict the behavior of auxetic foams during loading under different loading conditions.

Experimental curves of ν_{13} against the applied ε_{11} = *40* and *80%* for $\dot{\varepsilon}_{11}$ = *0.01* to *1* s^{-1} included three regions (i.e., three different patterns were recorded); (a) in the first region, the ν_{13} decreased with a rise in the applied strain until it reached its minimum amount [33], [35]. This was attributed to the opening of the microcell's walls that had been buckled in the thermo-mechanical process of converting a conventional foam to an auxetic; (b) in the second region, the ν_{13} raised with strain, returning to a conventional foam with a positive ν_{13} at strains between *18* and *20%*. In this domain,

microcells continued to open and converted to a rectangle-like shape; (c) the third zone, starting from a strain of about *40%*, showed an almost unchanged ν_{13} up to the final strain of *80%* as the cells' structure did not alter. However, for conventional foam, just two regions were seen [20]; i.e., the second and third ones. In other words, by increasing ε_{11} for regular foams the foam's ν_{13} goes towards higher values, and after a specific ε_{11} (near *50%*) reaches a plateau region.

In dynamic loading ($\dot{\varepsilon}_{11}$ = *5 s^{-1}*), however, the foam's ν_{13} began with a positive value which means the foam at this $\dot{\varepsilon}_{11}$ did not show an auxetic behavior, raising with a constant slope until the microcells became rectangular, and after that (i.e., a ε_{11} of about *20%*), the ν_{13} did not change with a further increase in the applied strain. This behavior is believed to be due to the time-dependent deformation of foam cells which is related to the foam's cell size [36]. Because $\dot{\varepsilon}_{11}$ accelerates the process the buckled cell's walls go to the straight alignment, this transition occurs in a shorter time, and the ε_{11} is smaller than under low $\dot{\varepsilon}_{11}$ ($\dot{\varepsilon}_{11}$ = *0.01* to *1*) loading conditions [24].

Statistical analysis showed that both ε_{11} and $\dot{\varepsilon}_{11}$ had significant influences on the foam Poisson's ratio, consistent with previous observations for compressive loading [29]. In addition, the interaction of ε_{11} and $\dot{\varepsilon}_{11}$ played a pivotal role in variations of ν_{13} during loading. In this regard, the interaction of ε_{11} and $\dot{\varepsilon}_{11}$ in the lower rates (i.e., *0.01* and *1 s^{-1}*) was more pronounced as, at these rates of loading, the microcells had more time to respond, which was not possible at the loading rate of *5 s^{-1}*.

The study for TSA shows that in addition to the ε_{11}, the $\dot{\varepsilon}_{11}$ also has an important effect in determining the ε_{11} domain that foam has an NPR. The interesting

finding is that by increasing the $\dot{\varepsilon}_{11}$, the effect of interaction between ε_{11} and $\dot{\varepsilon}_{11}$ on the TSA would decrease due to the same reason mentioned for ν_{13} in the former paragraph.

The FEM developed can be used to predict variations of ν_{13} and ν_{12} under tensile loading conditions in the regimes of loading rates like those examined in this study, i.e., the model shall be needed to be calibrated for high loading rates such as impact loading and compressive loading circumstances. In other words, the proposed model is an orthotropic model based on Hook's law, which was validated by the stress-strain curve in the direction of loading. Furthermore, for the model to account for non-linear deformations more accurately, a suitable hyperplastic material model (e.g., Fung) will be required. Such a model needs calibration for its coefficients by a significant number of experiments though. The model verification and validation were done by comparing the deformation during loading between the model and experiments (see Figure 16). Test class A (see Table 1) was used for verification and the model had more than *90%* correlation with experiments. Model validation was done by test class C (see Table 1), and the model had more than *80%* correlation with experiments.

5- Conclusions

In conclusion, an attempt was made to gain a better insight into the behavior of auxetic foams under different tensile load conditions. Microcells' deformations were found to change during loading, thus altering the ν_{13} value with increasing the applied strain. This behavior markedly differed when the applied loading rate was elevated. A load-rate dependent FE code was developed to incorporate these effects. The model was then successfully used to predict variations of ν_{13} in different loading conditions,

but in ranges like those employed for the model's calibration. The results of this study show that desired auxetic-structure properties strongly depend on the magnitude of applied deformations and loading rates. This must indeed be considered in designing such materials/structures for different applications.

References

[1] Lakes, R., "Foam structures with a negative poisson's ratio," *Science (1979)*, (1987), DOI: 10.1126/science.235.4792.1038.

[2] Jiang, Y., Z. Liu, N. Matsuhisa, *et al.*, "Auxetic Mechanical Metamaterials to Enhance Sensitivity of Stretchable Strain Sensors," *Advanced Materials*, (2018), DOI: 10.1002/adma.201706589.

[3] Airoldi, A., P. Bettini, P. Panichelli, *et al.*, "Chiral topologies for composite morphing structures – Part II: Novel configurations and technological processes," *Phys Status Solidi B Basic Res*, (2015), DOI: 10.1002/pssb.201584263.

[4] Airoldi, A., P. Bettini, P. Panichelli, *et al.*, "Chiral topologies for composite morphing structures – Part I: Development of a chiral rib for deformable airfoils," *Phys Status Solidi B Basic Res*, (2015), DOI: 10.1002/pssb.201451689.

[5] Zhu, Y., S. Jiang, Q. Zhang, *et al.*, "A novel monoclinic auxetic metamaterial with tunable mechanical properties," *Int J Mech Sci*, vol. 236, p. 107750, (2022), DOI: 10.1016/J.IJMECSCI.2022.107750.

[6] Zhang, X. Y., X. Ren, X. Y. Wang, *et al.*, "A novel combined auxetic tubular structure with enhanced tunable stiffness," *Compos B Eng*, vol. 226, p. 109303, (2021), DOI: 10.1016/J.COMPOSITESB.2021.109303.

[7] Prawoto, Y., "Seeing auxetic materials from the mechanics point of view: A structural review on the negative Poisson's ratio," *Comput Mater Sci*, (2012), DOI: 10.1016/j.commatsci.2012.02.012.

[8] Hou, F., S. Xiao, and H. Wang, "Mechanical properties characterization and zero Poisson's ratio design for perforated auxetic metamaterial by computational homogenized method," *Mechanics of Advanced Materials and Structures*, vol. 29, no. 28, pp. 7640–7651, (2022), DOI: 10.1080/15376494.2021.2004268.

[9] Ha, C. S., M. E. Plesha, and R. S. Lakes, "Chiral three-dimensional lattices with tunable Poisson's ratio," *Smart Mater Struct*, (2016), DOI: 10.1088/0964-1726/25/5/054005.

[10] Kim, J. S., M. Mahato, J. H. Oh, *et al.*, "Multi-Purpose Auxetic Foam with Honeycomb Concave Micropattern for Sound and Shock Energy

Absorbers," *Adv Mater Interfaces*, vol. 10, no. 4, p. 2202092, (2023), DOI: 10.1002/ADMI.202202092.

[11] Tahir, D., M. Zhang, and H. Hu, "Auxetic Materials for Personal Protection: A Review," *physica status solidi (b)*, vol. 259, no. 12, p. 2200324, (2022), DOI: 10.1002/PSSB.202200324.

[12] Hamzehei, R., S. Rezaei, J. Kadkhodapour, *et al.*, "2D triangular anti-trichiral structures and auxetic stents with symmetric shrinkage behavior and high energy absorption," *Mechanics of Materials*, (2020), DOI: 10.1016/j.mechmat.2019.103291.

[13] Wu, W., Y. Liu, J. Yan, *et al.*, "Blast performance of polyurethane foam-filled auxetic honeycomb sandwich beams," *Compos Struct*, vol. 338, p. 118104, (2024), DOI: 10.1016/J.COMPSTRUCT.2024.118104.

[14] Etemadi, E., M. Zhang, M. Gholikord, *et al.*, "Quasi-static and dynamic behavior analysis of 3D CFRP woven laminated composite auxetic structures for load-bearing and energy absorption applications," *Compos Struct*, vol. 340, p. 118182, (2024), DOI: 10.1016/J.COMPSTRUCT.2024.118182.

[15] Haque Faisal, N., L. Scott, F. Booth, *et al.*, "Effect of fillers on compression loading performance of modified re-entrant honeycomb auxetic sandwich structures," *Journal of Strain Analysis for Engineering Design*, vol. 58, no. 2, pp. 98–117, (2023), DOI: 10.1177/03093247221083210/ASSET/IMAGES/LARGE/10.1177_03093247221083210-FIG15.JPEG.

[16] Duncan, O., T. Shepherd, C. Moroney, *et al.*, "Review of auxetic materials for sports applications: Expanding options in comfort and protection," (2018). DOI: 10.3390/app8060941.

[17] Casavola, C., L. Del Core, V. Moramarco, *et al.*, "Full-field mechanical characterization of polyurethane foams under large deformations by digital image correlation," *Mechanics of Advanced Materials and Structures*, vol. 29, no. 24, pp. 3540–3555, (2022), DOI: 10.1080/15376494.2021.1905915.

[18] Koohbor, B., G. Youssef, K. Z. Uddin, *et al.*, "Dynamic Behavior and Impact Tolerance of Elastomeric Foams Subjected to Multiple Impact Conditions," *Journal of Dynamic Behavior of Materials*, vol. 8, no. 3, pp. 359–370, (2022), DOI: 10.1007/S40870-022-00340-Z/METRICS.

[19] Casavola, C., L. Del Core, V. Moramarco, *et al.*, "Experimental and numerical analysis of the Poisson's ratio on soft polyurethane foams under tensile and cyclic compression load," *Mechanics of Advanced Materials and Structures*, vol. 29, no. 28, pp. 7172–7188, (2022), DOI: 10.1080/15376494.2021.1994061.

[20] Widdle, R. D., A. K. Bajaj, and P. Davies, "Measurement of the Poisson's ratio of flexible polyurethane foam and its influence on a uniaxial

compression model," *Int J Eng Sci*, vol. 46, no. 1, (2008), DOI: 10.1016/j.ijengsci.2007.09.002.

[21] Scarpa, F., P. Pastorino, A. Garelli, *et al.*, "Auxetic compliant flexible PU foams: Static and dynamic properties," *Phys Status Solidi B Basic Res*, vol. 242, no. 3, pp. 681–694, (2005), DOI: 10.1002/pssb.200460386.

[22] Wang, Y. C., R. Lakes, and A. Butenhoff, "Influence of Cell Size on Re-Entrant Transformation of Negative Poisson's Ratio Reticulated Polyurethane Foams," *https://doi.org/10.1177/026248930102000601*, vol. 20, no. 4–6, pp. 373–385, (2001), DOI: 10.1177/026248930102000601.

[23] Zhang, Q., F. Scarpa, D. Barton, *et al.*, "Impact properties of uniaxially thermoformed auxetic foams," *Int J Impact Eng*, vol. 163, p. 104176, (2022), DOI: 10.1016/J.IJIMPENG.2022.104176.

[24] Boumdouha, N. and M. A. Louar, "Influence of Microstructure on the Dynamic Behaviour of Polyurethane Foam with Various Densities," *Journal of Basic & Applied Sciences*, vol. 19, pp. 131–150, (2023), DOI: 10.29169/1927-5129.2023.19.12.

[25] Wu, C., G. Ye, Y. Zhao, *et al.*, "Experimental and numerical study of in-plane uniaxial compression response of PU foam filled aluminum arrowhead auxetic honeycomb," *Rapid Prototyp J*, vol. 30, no. 3, pp. 502–512, (2024), DOI: 10.1108/RPJ-08-2023-0267/FULL/PDF.

[26] Srivastava, C., V. Mahesh, P. Pitchai, *et al.*, "Effective Mechanical Properties of Auxetic Materials: Numerical Predictions Using Variational Asymptotic Method Based Homogenization," *Journal of Applied Mechanics, Transactions ASME*, vol. 90, no. 11, (2023), DOI: 10.1115/1.4062845/7021552/JAM-23-1174.PDF.

[27] Koohbor, B., A. Blourchian, K. Z. Uddin, *et al.*, "Characterization of Energy Absorption and Strain Rate Sensitivity of a Novel Elastomeric Polyurea Foam," *Adv Eng Mater*, vol. 23, no. 1, p. 2000797, (2021), DOI: 10.1002/ADEM.202000797.

[28] Koohbor, B., N. K. Singh, and A. Kidane, "Radial and axial inertia stresses in high strain rate deformation of polymer foams," *Int J Mech Sci*, vol. 181, p. 105679, (2020), DOI: 10.1016/J.IJMECSCI.2020.105679.

[29] Zhai, X., J. Gao, H. Liao, *et al.*, "Mechanical behaviors of auxetic polyurethane foam at quasi-static, intermediate and high strain rates," *Int J Impact Eng*, vol. 129, no. March, pp. 112–118, (2019), DOI: 10.1016/j.ijimpeng.2019.03.002.

[30] Novak, N., M. Vesenjak, S. Tanaka, *et al.*, "Compressive behaviour of chiral auxetic cellular structures at different strain rates," *Int J Impact Eng*, vol. 141, no. March, (2020), DOI: 10.1016/j.ijimpeng.2020.103566.

[31] Duncan, O., N. Bailly, T. Allen, *et al.*, "Effect of compressive strain rate on auxetic foam," *Applied Sciences (Switzerland)*, vol. 11, no. 3, (2021), DOI: 10.3390/app11031207.

[32] Abedini, N. H. Z., A. Nourani, M. Mohseni, *et al.*, "Effects of geometrical and processing parameters on mechanical properties of auxetic polyurethane foams," *SN Appl Sci*, vol. 4, no. 6, (2022), DOI: 10.1007/S42452-022-05042-8.

[33] Zhang, Q., F. Scarpa, D. Barton, *et al.*, "Impact properties of uniaxially thermoformed auxetic foams," *Int J Impact Eng*, vol. 163, p. 104176, (2022), DOI: 10.1016/J.IJIMPENG.2022.104176.

[34] Wang, X., K. Jia, Y. Liu, *et al.*, "In-Plane Impact Response of Graded Foam Concrete-Filled Auxetic Honeycombs," *Materials 2023, Vol. 16, Page 745*, vol. 16, no. 2, p. 745, (2023), DOI: 10.3390/MA16020745.

[35] Zhang, Q., W. Lu, F. Scarpa, *et al.*, "Topological characteristics and mechanical properties of uniaxially thermoformed auxetic foam," *Mater Des*, vol. 211, p. 110139, (2021), DOI: 10.1016/J.MATDES.2021.110139.

[36] Pastorino, P., F. Scarpa, S. Patsias, *et al.*, "Strain rate dependence of stiffness and Poisson's ratio of auxetic open cell PU foams," *Phys Status Solidi B Basic Res*, vol. 244, no. 3, pp. 955–965, (2007), DOI: 10.1002/pssb.200572714.

Tables caption list:

1. Table 1: Testing table which categorizes experiments based on the purpose of testing and loading conditions.
2. Table 2: Material property of auxetic foam.

Tables:

Table 1:

Testing class and purpose	Case No.	ε_{11}	$\dot{\varepsilon}_{11}$
A: conventional foams (control tests) Purpose: comparison with auxetic foams	1	10	0.01
	2	40	0.01
	3	80	0.01
	4	10	0. 1
	5	40	0.1
	6	80	0.1
	7	10	1
	8	40	1
	9	80	1
	10	10	5
	11	40	5
	12	80	5
B: Calibration auxetic foams	1	10	0.01

Purpose: finding ν behavior in different loading conditions and developing FEM	2 3 4 5 6 7 8 9 10 11 12	40 80 10 40 80 10 40 80 10 40 80	0.01 0.01 0.1 0.1 0.1 1 1 1 5 5 5
C: Validation auxetic foams Purpose: examining the capability of the model to predict the behavior of auxetic foams at different loading conditions	1 2 3 4 5 6 7 8 9	10 40 80 10 40 80 10 40 80	0.05 0.05 0.05 0.5 0.5 0.5 2.5 2.5 2.5

Table 2:

Mechanical Property	Quantity
ρ	20 $\frac{\text{kg}}{\text{m}^3}$
E_1	170 MPa
E_2	170 MPa
E_3	150 MPa
G_{12}	420 MPa
G_{13}	520 MPa
G_{23}	420 MPa

Figures caption list:

1. Figure 1: a) Schematic of the specimen of *ASTM D-3574 Test E*. b) The pressure mechanism and the specimens.
2. Figure 2: a) The test setup shows the light source, digital camera, and specimen attached to the fixture. b) Experimental set-up to ensure uniform loading during testing.
3. Figure 3: FEM of the test specimen a) Boundary conditions and loading. b) Element size.
4. Figure 4: The flowchart showing the procedure performed to develop an adaptive user-defined material (UMAT) FEM code based on the outputs of experiments.

5. Figure 5: a) Conventional foam with honeycomb cells. b) Temperature-time graph of the thermo-mechanical process. c) Auxetic foam with buckled honeycomb[32].
6. Figure 6: a) Conventional foam with honeycomb cells and thickness of the specimen. b) Auxetic foam with buckled honeycomb cells and thickness of the specimen. PG, T, A, and L represent the words polygon, thickness, area, and perimeter, respectively.
7. Figure 7: Variation of ν_{13} for conventional foams at different loading conditions. a) ε_{11}=*10%*. b) ε_{11} = *40%*. c) ε_{11} = *80%*.
8. Figure 8: Mechanical property of auxetic foam. a) Stress-strain curve for the auxetic foam with $\dot{\varepsilon}_{11}$ = *0.01 s*$^{-1}$. b) Variations of ν for the nonauxetic direction of foam at ε_{11} = *80%* and $\dot{\varepsilon}_{11}$ = *0.01 s*$^{-1}$ And compare their ν magnitude and trend with conventional foam.
9. Figure 9: Variations of ν_{13} for auxetic foams under different loading conditions. The ν_{13} first has a negative value which goes to a positive value, and at the final stage, it reaches a constant value until the end of loading. So, according to the image processing findings, variations of ν_{13} to ε_{11}. a) for ε_{11}= *10%*. b) for ε_{11}= *40%*. c) for ε_{11}= *80%*.
10. Figure 10*:* The blue line represents variations of ν_{13} for a) $\dot{\varepsilon}_{11}$= *0.01 s*$^{-1}$, b) $\dot{\varepsilon}_{11}$ = *0.1 s*$^{-1}$, c) $\dot{\varepsilon}_{11}$= *1 s*$^{-1}$, d) $\dot{\varepsilon}_{11}$= *5 s*$^{-1}$, recorded during experiments. The red line indicates the TSA region; the black dashed line is the curve fitted on the experiment's curve (see sec 3.7).
11. Figure 11: ν_{13} measured for different loading conditions.
12. Figure 12: The ANOVA to investigate the effect of the loading parameter on the ν. a) Main effects Plot for ν which indicates that The ε_{11} has the most effect on the ν from ε_{11} = *10* to *40%*, on the other hand, *The* $\dot{\varepsilon}_{11}$ has the most effect on the ν between the $\dot{\varepsilon}_{11}$ =*1* to *5 s*$^{-1}$. b) Interaction plot for ν that shows the interaction between ε_{11} and $\dot{\varepsilon}_{11}$ had the most effect on the loading condition of $\dot{\varepsilon}_{11}$ = *0.01 s*$^{-1}$ and ε_{11} = *40%*, while the least effect was observed at loading conditions of $\dot{\varepsilon}_{11}$ = *5 s*$^{-1}$ and ε_{11} = *40%*.
13. Figure 13: Transient strain auxeticity (TSA) measured for different loading conditions. No TSA was observed for ε_{11} = *10%* and all strains for $\dot{\varepsilon}_{11}$ = *5 s*$^{-1}$.
14. Figure 14: a) Main effects plot for transient strain auxeticity (TSA). By increasing the quantity of ε_{11}, the amount of TSA is decreased. By increasing the $\dot{\varepsilon}_{11}$ amount of TSA decreased dramatically. b) Interaction effect on the ν. Interaction in the load case with $\dot{\varepsilon}_{11}$ = *0.01 s*$^{-1}$ has the most effect, and the load case with $\dot{\varepsilon}_{11}$= *5 s*$^{-1}$ has the least effect on the changing ν.
15. Figure 15: Comparison of FEM results and measured Poisson's ratios at the loading rate of a) *0.05 s*$^{-1}$ (auxetic direction, R-square = *87%*, non-auxetic direction, R-square = *80%*), b) *0.5 s*$^{-1}$ (auxetic direction, R-square = *83%*, non-auxetic direction R-square = *85%*).

16. Figure 16: Displacement vectors for the adaptive Hook's model and compare with experiments data for model validation.

Nomenclature

E_1	Young's modulus in direction 1
E_2	Young's modulus in direction 2
E_3	Young's modulus in direction 3
G_{12}	Shear modulus in plane 12
G_{13}	Shear modulus on plane 13
G_{23}	Shear modulus in plane 23
x^0	FEM initial parameters ($\nu_0, \varepsilon_{11}, \dot{\varepsilon}_{11}$)
x^{sol}	FEM outputs ($\nu, stress, strain$)
ε_{11}	Normal strain in direction 1
ε_{22}	Normal strain in direction 2
ε_{33}	Normal strain in direction 3
ε_{12}	Shear strain in plane 12
ε_{13}	Shear strain in plane 13
ε_{23}	Shear strain in plane 23
$\dot{\varepsilon}$	Loading rate
$\dot{\varepsilon}_{11}$	Loading rate in direction 1

σ_{11}	Normal stress in direction 1
σ_{22}	Normal stress in direction 1
σ_{33}	Normal stress in direction 1
σ_{12}	Shear stress on plane 12
σ_{13}	Shear stress on plane 13
σ_{23}	Shear stress on plane 23
σ_{uniax}	Uniaxial stress
ν_0	Initial Poisson's ratio
ν_{12}	Poisson's ratio corresponding to loading in direction 1 and strain in direction 2
ν_{21}	Poisson's ratio corresponding to loading in direction 2 and strain in direction 1
ν_{13}	Poisson's ratio corresponding to loading in direction 1 and strain in direction 3
ν_{31}	Poisson's ratio corresponding to loading in direction 3 and strain in direction 1
ν_{23}	Poisson's ratio corresponding to loading in direction 2 and strain in direction 3
ν_{32}	Poisson's ratio corresponding to loading in direction 3 and strain in direction 2

Amir Nourani joined the Department of Mechanical Engineering at Sharif University of Technology in 2018. Amir obtained his PhD from the University of Toronto, Canada, in 2016. He received his BSc and MSc degrees in Mechanical Engineering from Isfahan University of Technology, Iran. He is currently serving as an Associate Professor the at Sharif University of Technology. His research interests primarily focus on fracture

mechanics, orthopedic biomechanics, experimental solid mechanics, and the performance of metamaterials, such as auxetic materials.

Ali Behbahani received his Bachelor of Science in Mechanical Engineering from Shiraz University, Shiraz, Iran, in 2019. He then earned his Master of Science in Mechanical Engineering from Sharif University of Technology, Tehran, Iran in 2022. He is currently pursuing his PhD at the University of Tennessee, Knoxville, TN, USA in 2023. He is currently employed as a graduate research assistant at the University of Tennessee, Knoxville, where he focuses on research related to computational solid mechanics and metal 3D printing simulation.

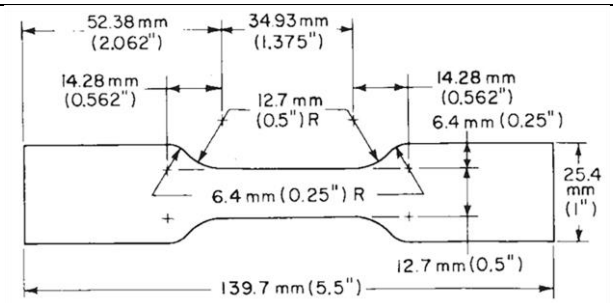

(a)

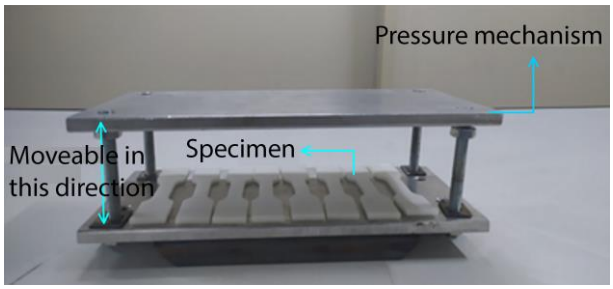

(b)

Figure 1

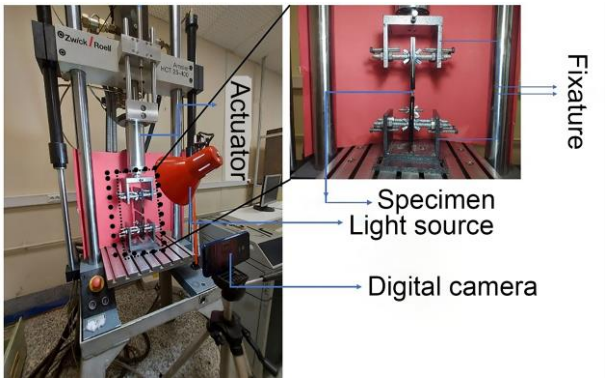
Actuator
Fixature
Specimen
Light source
Digital camera

(a)

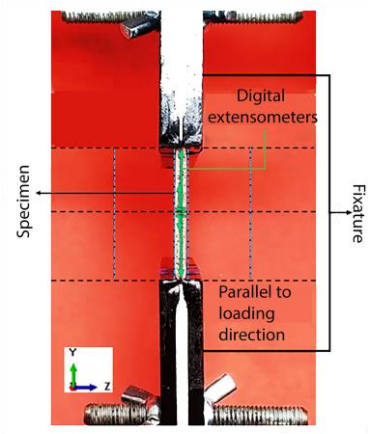
Digital extensometers
Specimen
Fixature
Parallel to loading direction
Y
Z

(b)

Figure 2

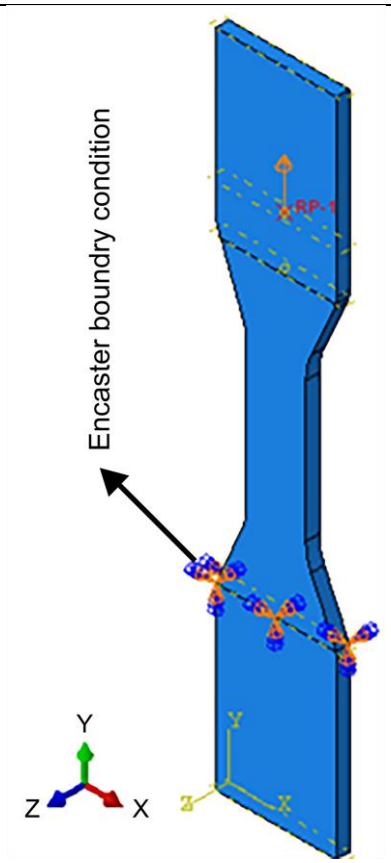

(a)

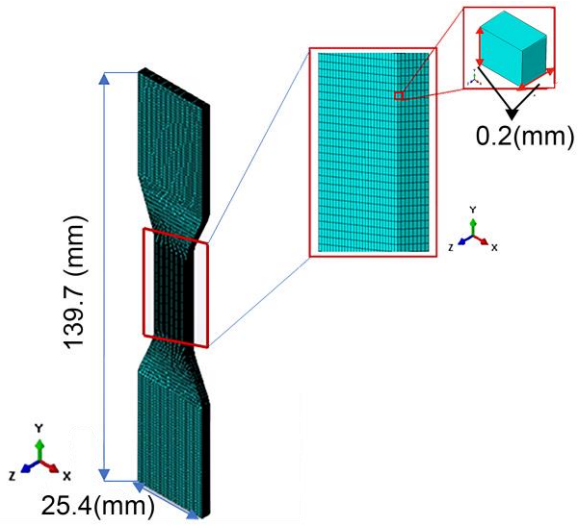

(b)

Figure 3

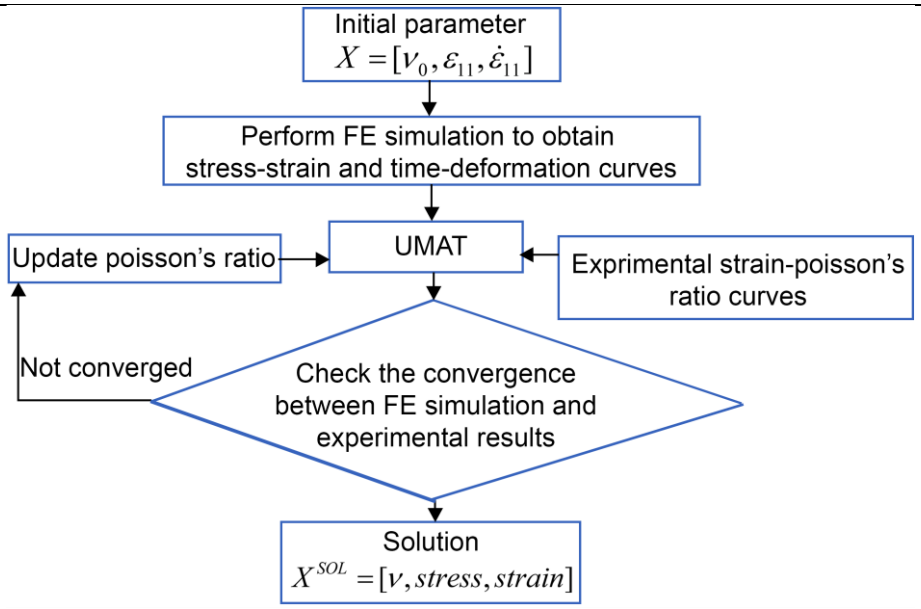

Figure 4

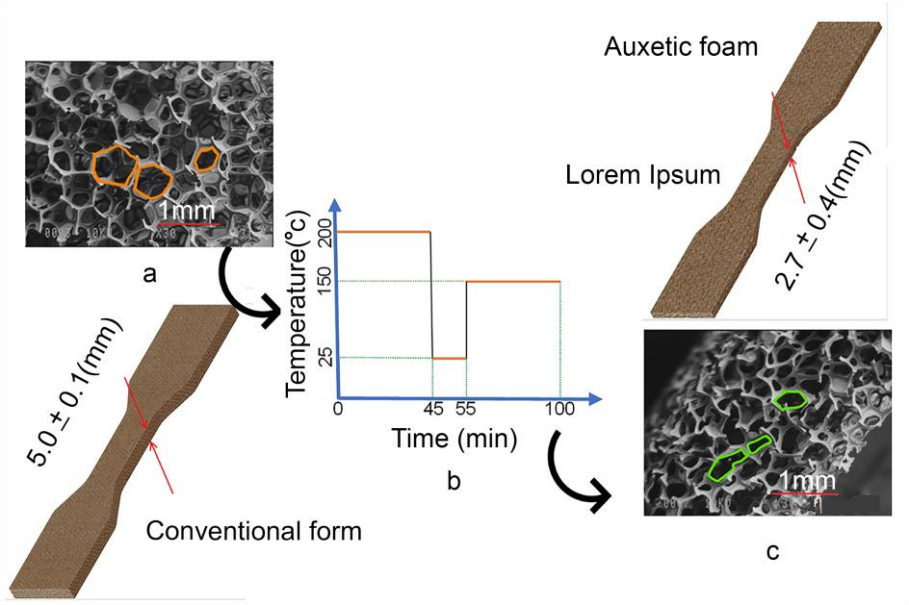

Figure 5

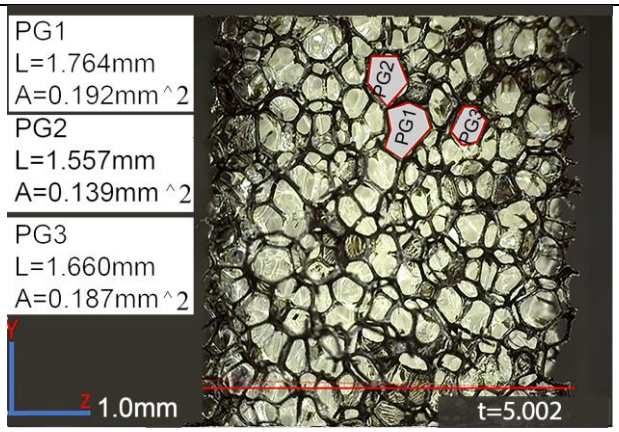
PG1
L=1.764mm
A=0.192mm^2
PG2
L=1.557mm
A=0.139mm^2
PG3
L=1.660mm
A=0.187mm^2
PG2
PG1
PG3
Y
Z
1.0mm
t=5.002

(a)

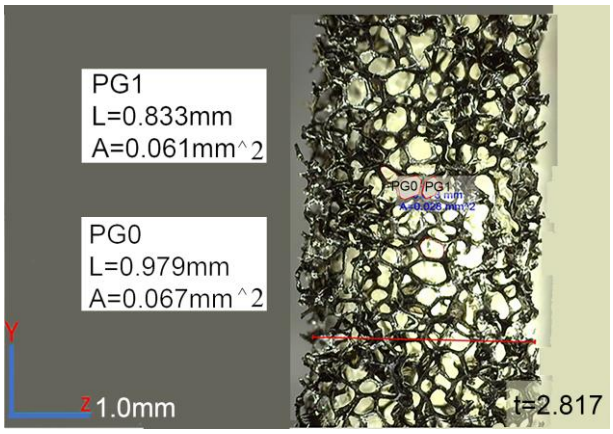
PG1
L=0.833mm
A=0.061mm^2
PG0
L=0.979mm
A=0.067mm^2
Y
Z
1.0mm
t=2.817

(b)

Figure 6

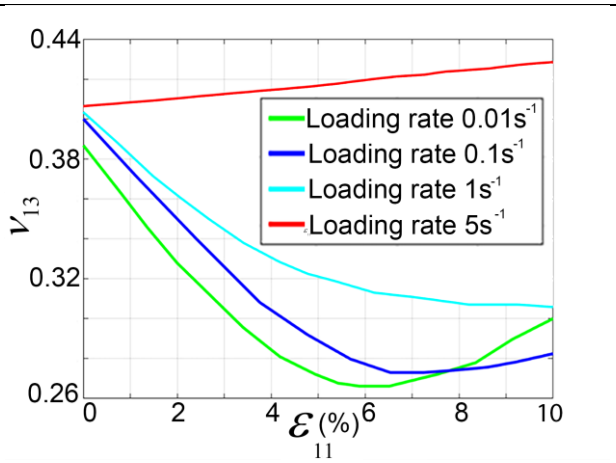
0.44
0.38
0.32
0.26
ν_{13}
0
2
4
6
8
10
ε_{11} (%)
Loading rate 0.01s^{-1}
Loading rate 0.1s^{-1}
Loading rate 1s^{-1}
Loading rate 5s^{-1}

(c)

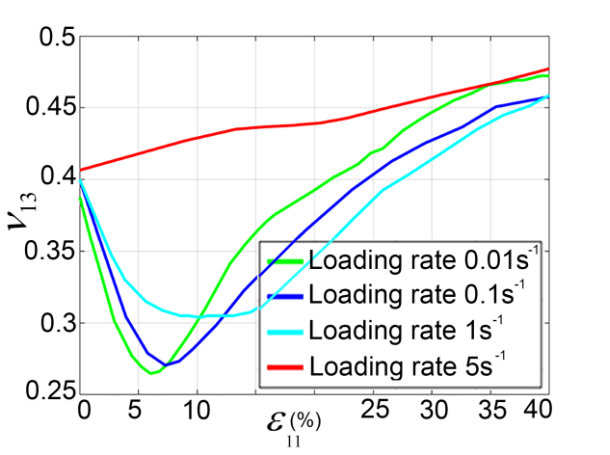
0.5
0.45
0.4
0.35
0.3
0.25
ν_{13}
0
5
10
25
30
35
40
ε_{11} (%)
Loading rate 0.01s^{-1}
Loading rate 0.1s^{-1}
Loading rate 1s^{-1}
Loading rate 5s^{-1}

(b)

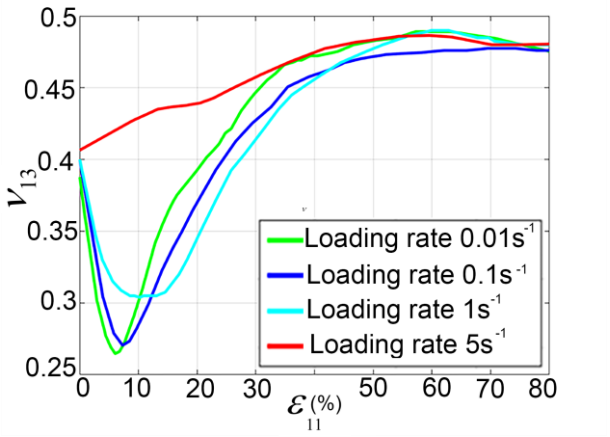
0.5
0.45
0.4
0.35
0.3
0.25
ν_{13}
0
10
20
30
50
60
70
80
ε_{11} (%)
Loading rate 0.01s^{-1}
Loading rate 0.1s^{-1}
Loading rate 1s^{-1}
Loading rate 5s^{-1}

(c)

Figure 7

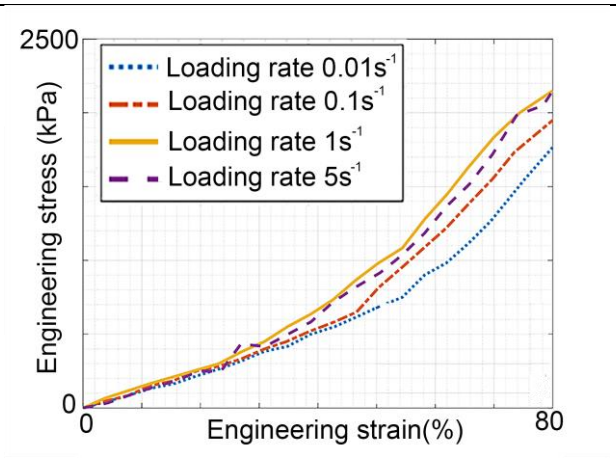
2500
0
0
80
Engineering stress (kPa)
Engineering strain(%)
Loading rate 0.01s-1
Loading rate 0.1s-1
Loading rate 1s-1
Loading rate 5s-1

(a)

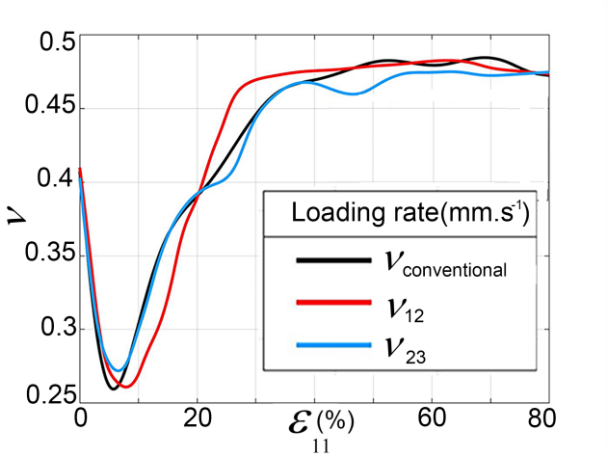
0.5
0.45
0.4
0.35
0.3
0.25
0
20
60
80
ε11(%)
ν
Loading rate(mm.s-1)
νconventional
ν12
ν23

(b)

Figure 8

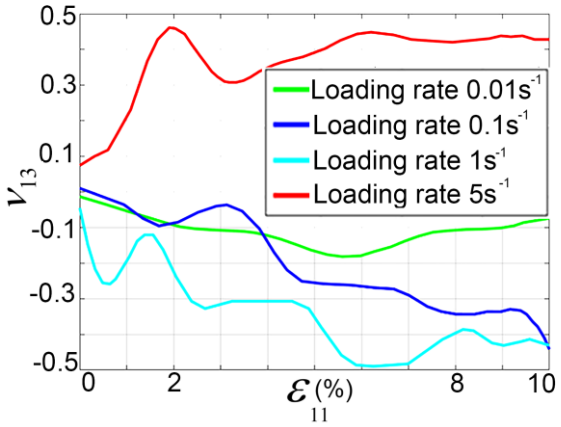
0.5
0.3
0.1
-0.1
-0.3
-0.5
0
2
8
10
ν_{13}
ε_{11} (%)
Loading rate 0.01s^{-1}
Loading rate 0.1s^{-1}
Loading rate 1s^{-1}
Loading rate 5s^{-1}

(a)

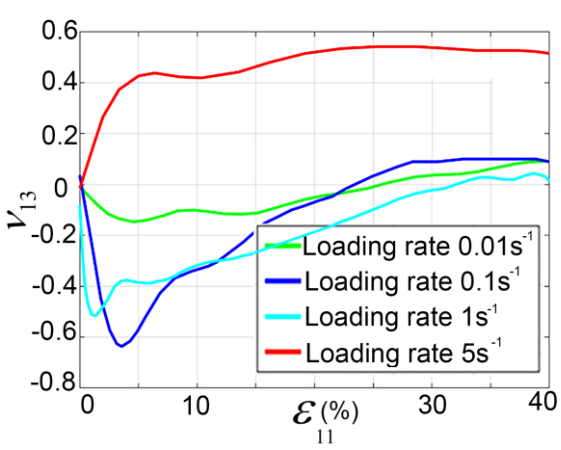
0.6
0.4
0.2
0
-0.2
-0.4
-0.6
-0.8
0
10
30
40
ν_{13}
ε_{11} (%)
Loading rate 0.01s^{-1}
Loading rate 0.1s^{-1}
Loading rate 1s^{-1}
Loading rate 5s^{-1}

(b)

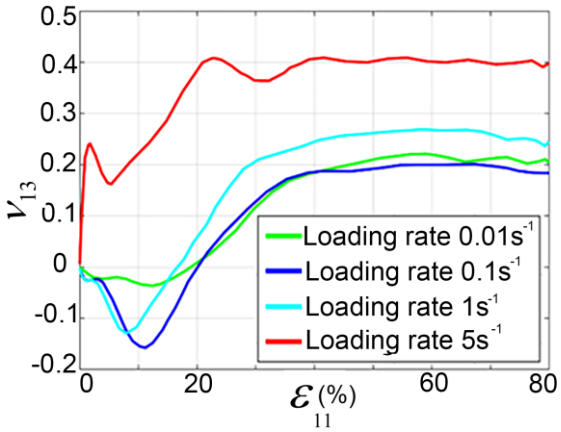
0.5
0.4
0.3
0.2
0.1
0
-0.1
-0.2
0
20
60
80
ν_{13}
ε_{11} (%)
Loading rate 0.01s^{-1}
Loading rate 0.1s^{-1}
Loading rate 1s^{-1}
Loading rate 5s^{-1}

(c)

Figure 9

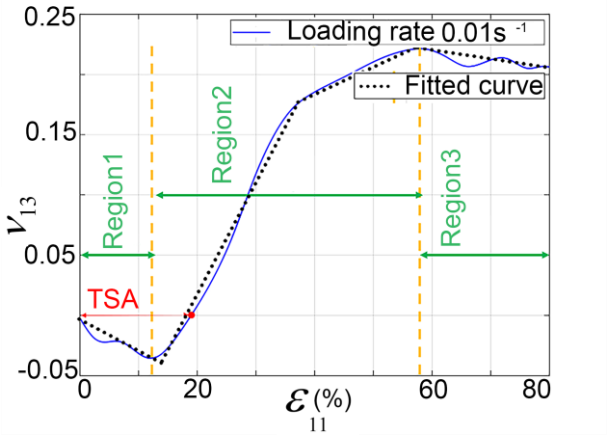
Loading rate 0.01s -1
Fitted curve
Region1
Region2
Region3
TSA
0.25
0.15
0.05
-0.05
0
20
60
80
ε_{11} (%)
ν_{13}

(a)

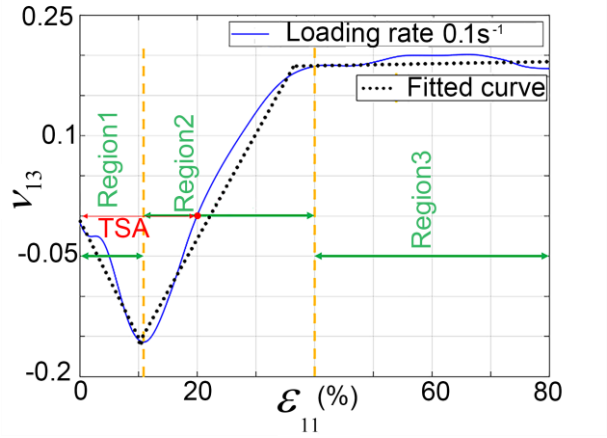
Loading rate 0.1s-1
Fitted curve
Region1
Region2
Region3
TSA
0.25
0.1
-0.05
-0.2
0
20
60
80
ε_{11} (%)
ν_{13}

(b)

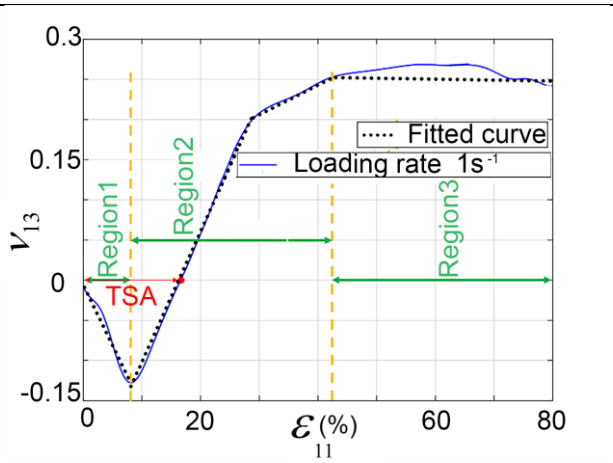
0.3
0.15
0
-0.15
0
20
60
80
ε_{11} (%)
ν_{13}
Region1
Region2
Region3
TSA
Fitted curve
Loading rate 1s^{-1}

(c)

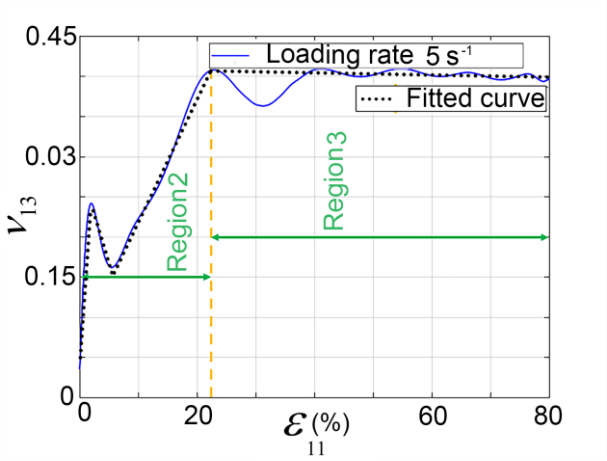
0.45
0.03
0.15
0
0
20
60
80
ε_{11} (%)
ν_{13}
Region2
Region3
Loading rate 5 s^{-1}
Fitted curve

(d)

Figure 10

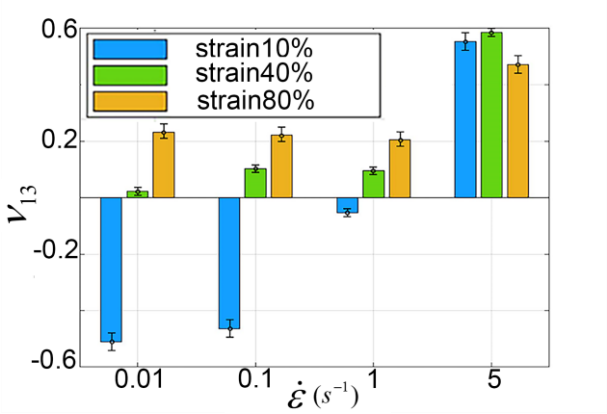
strain10%
strain40%
strain80%
0.6
0.2
-0.2
-0.6
ν_{13}
0.01
0.1
1
5
$\dot{\varepsilon}\ (s^{-1})$

Figure 11

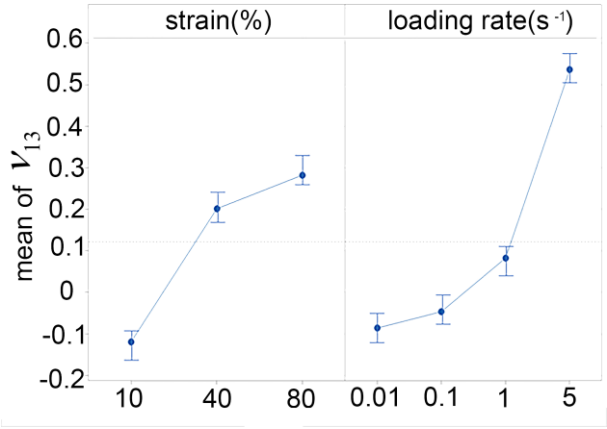
strain(%)
loading rate(s -1)
mean of ν_{13}
0.6
0.5
0.4
0.3
0.2
0.1
0
-0.1
-0.2
10
40
80
0.01
0.1
1
5

(a)

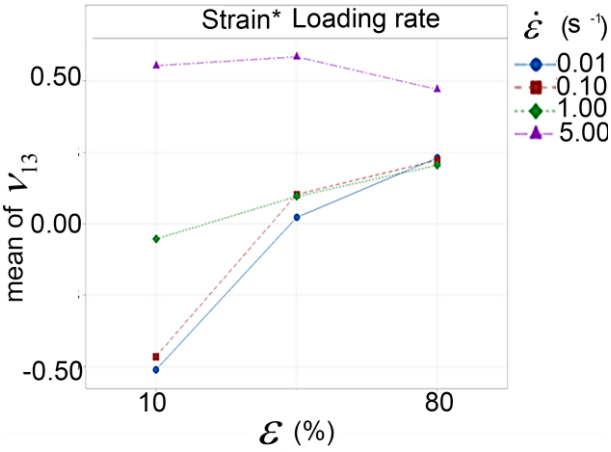
Strain* Loading rate
$\dot{\varepsilon}$ (s -1)
0.01
0.10
1.00
5.00
mean of ν_{13}
0.50
0.00
-0.50
10
80
ε (%)

(b)

Figure 12

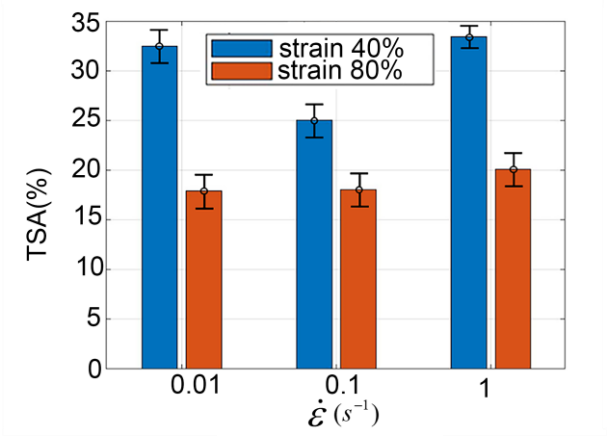

Figure 13

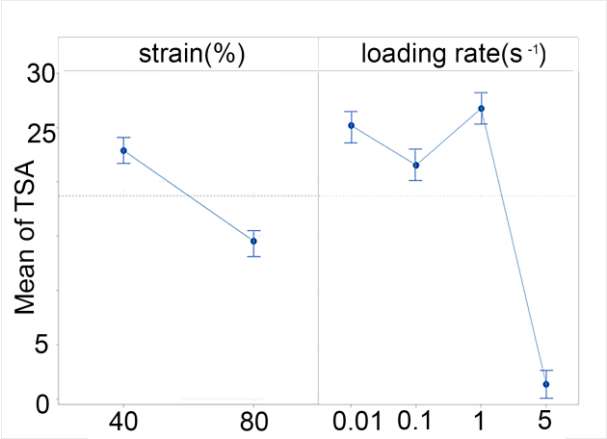

(a)

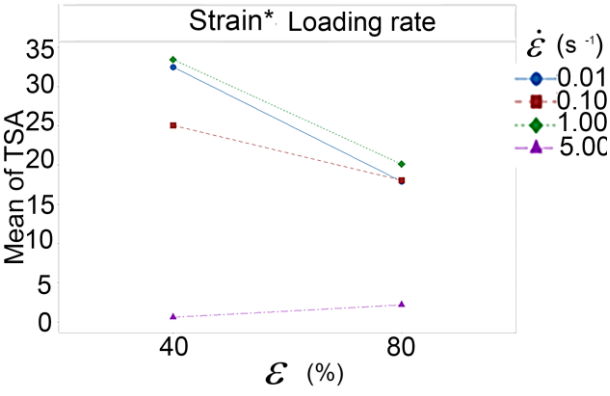

(b)

Figure 14

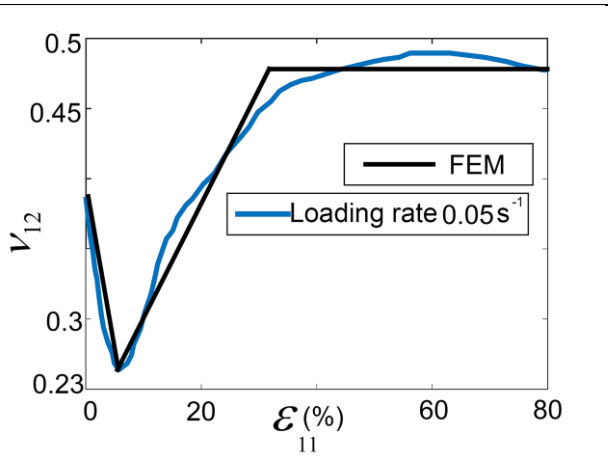
0.5
0.45
0.3
0.23
ν_{12}
FEM
Loading rate 0.05 s^{-1}
0
20
60
80
ε_{11} (%)

(a)

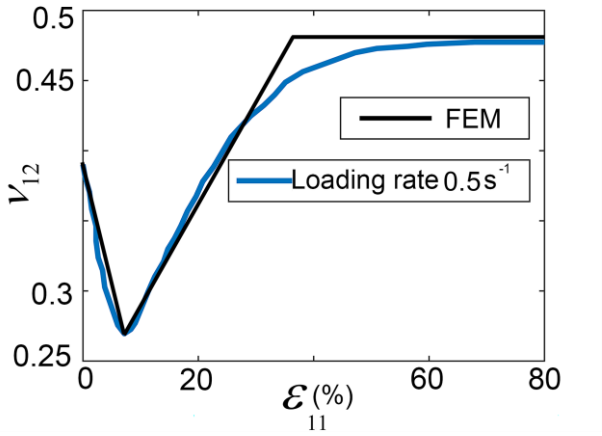
0.5
0.45
0.3
0.25
ν_{12}
FEM
Loading rate 0.5 s^{-1}
0
20
60
80
ε_{11} (%)

(b)

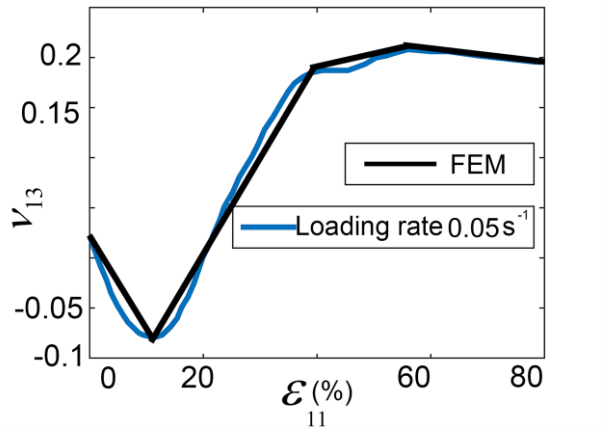
0.2
0.15
-0.05
-0.1
ν_{13}
FEM
Loading rate 0.05 s^{-1}
0
20
60
80
ε_{11} (%)

(c)

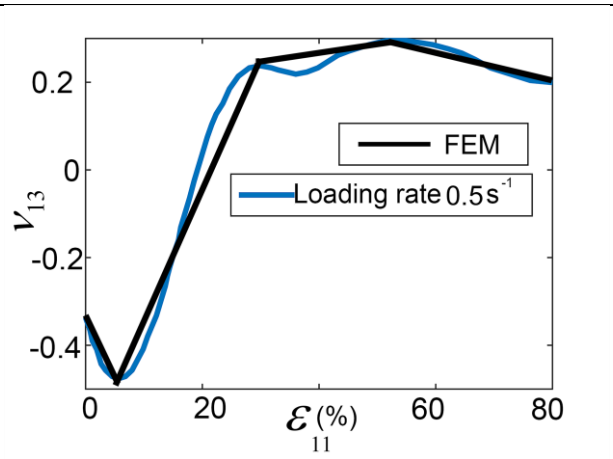

(d)

Figure 15

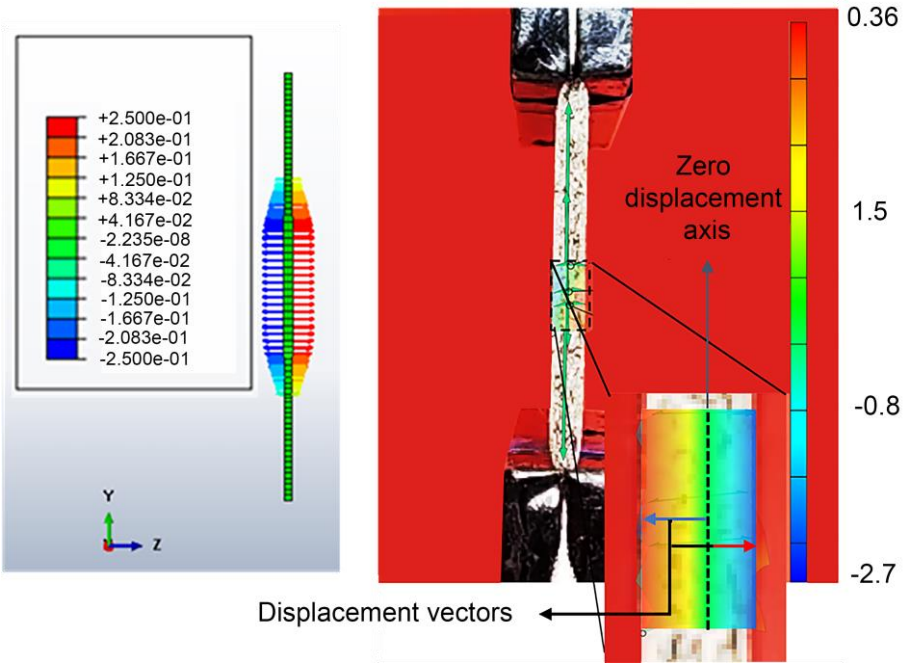

Figure 16